ARTICLE

Enhanced Photoluminescence and Photoconductivity of ZnO Nanowires with Sputtered Zn

A. Bera, T. Ghosh, and D. Basak*

Department of Solid State Physics, Indian Association for the Cultivation of Science, Jadavpur, Kolkata 700032, India

ABSTRACT We have sputtered Zn onto quasi-one-dimensional ZnO nanowires (NWs) in order to investigate the effect of Zn diffusion on the photoluminescence and photoconduction properties of ZnO NWs. Elemental mapping clearly indicates higher Zn concentration in the NWs due to diffusion of Zn. The Zn-sputtered NWs show an enhanced ultraviolet emission with 7 nm red shift. Since the ionization energy of Zn_i is 51 meV, the enhanced PL emission with a red shift is corelated to the coupling between free exciton and zinc interstitials (Zn_i) defects. The photocurrent transients show almost 20 times more photocurrent generation in Zn/ZnO NWs compared to the as-grown NWs. In contrast, the thin film shows no significant change in the photoluminescence and photoconductivity. Based on the photoconductivity and photoluminescence results, we predict that Zn diffusion in the NWs occurs easily compared to the films because of the smaller dimensions of the NWs.

KEYWORDS: ZnO • Zn interstitial • photoluminescence • photoconductivity • sputtering

INTRODUCTION

Wide band gap of 3.37 eV, a large excitonic binding energy of 60 meV, and easy growth at low cost make ZnO a promising material for nanoscale device applications. Vertically aligned ZnO nanowires (NWs) have already shown a variety of astonishing applications in optoelectronic and electromechanical nanodevices, such as solar cells (1), UV detectors (2), UV lasers (3), light emitting diodes (4), and piezo-nanogenerators (5). However, in general, the performance of a device depends strongly on the material quality which again depends on the size, shape and emission characteristics of the materials at room temperature (6). For example, ZnO may show quite different photoconducting property when grown in the form of nanocrystalline thin film and NWs array. ZnO thin films grown with highly oriented crystallites along (002) direction do not show significant photoconductivity (7, 8), whereas vertically grown NWs arrays (9, 10) exhibit high UV photoconductivity. Because UV photoconductivity in ZnO is highly a surface controlled process, high surface-to-volume ratio of the NWs compared to the thin film makes the former highly sensitive to UV photons. Therefore, nanostructured ZnO is not only very promising for nano-optoelectronic devices but also useful for studying the fundamental properties as compared to thin films although the reproducibility might be higher when working with the thin films. This explains the reason behind an intensive research for controlling and manipulating nanostructured ZnO by understanding the defects and their role on the material properties. ZnO contains large number of intrinsic and extrinsic defects. It has been believed for a long time that zinc interstitial (Zn_i) is the dominant defects that causes the n-type conductivity in ZnO (11, 12). Also few recent reports predict that the conductivity comes from the hydrogen-related defects (13, 14). A controversy regarding the origin of n-type conductivity still prevails while scientists put forward various results in support of low and high formation energies of the intrinsic defects in oxygen or zinc rich conditions including the formation of complex defects (15, 16). However, the presence of such defect states largely affects the photoluminescence and photoconductivity of ZnO. ZnO annealing in oxygen rich or oxygen deficient ambient have been reported in order to remove or increase the oxygen vacancy (V_O) type of defects by studying the photoluminescence (17, 18) and photoconduction properties (19, 20). Experiments to introduce additional Zn in ZnO have been carried by thermal evaporation of Zn on ZnO (21), and sputtering Zn in between two ZnO:Al thin film layers (22). No attempt has been made to introduce extra Zn in low-dimensional, i.e., NWs of ZnO where different Zn diffusion mechanism is expected. Therefore, in this article, we have sputtered excess Zn onto aqueous chemically grown (ACG) ZnO NWs' surface by DC sputtering at 400 °C and investigated the effect of excess Zn on the photoluminescence and photoconduction properties by comparing these with the bare ZnO NWs. Interestingly, we have observed that the near band-edge emission of ZnO NWs is enhanced by 6 times and the photocurrent generation is increased 20 times compared to as-grown NWs. We correlate the enhancement of both the UV emission and response due to the coupling between the free exciton (FX) and the interstitial Zn.

EXPERIMENTAL SECTION

The ZnO NWs grown on the glass substrates following the ACG method as described elsewhere (9). In brief, we first

* Corresponding author. E-mail: sspdb@iacs.res.in. Fax: (91)-(33) 24732805.
Received for review July 10, 2010 and accepted September 21, 2010

DOI: 10.1021/am1006047

Published on Web 10/04/2010

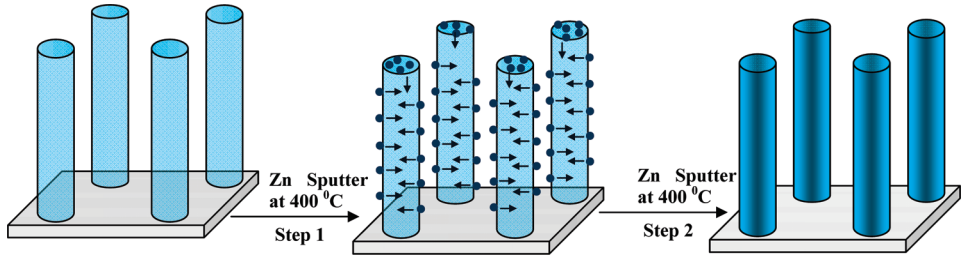

FIGURE 1. Model showing the mechanism of Zn diffusion at 400 °C by DC magnetron sputtering technique.

deposited a ZnO seed layer by coating with a solution of zinc acetate and thermally decomposing it at 350 °C. Then the NWs were grown by dipping the substrates with the seed layer in an equimolar mixture of $(CH_3COO)_2Zn \cdot 2H_2O$ and hexamethylenetetramine $(CH_2)_6N_4$ (20 mM) in deionized water at 90 °C for 1 h. The substrates were then removed from the solution, rinsed in deionized water and dried. ZnO thin films of thickness 200 nm were deposited using a ZnO target (MTI Corporation. USA 99.99%) by RF sputtering technique keeping the substrate temperature 500 °C at 100 W RF power with argon and oxygen gas flow rate of 20 SCCM each. The ZnO NWs arrays and the thin films were loaded in a DC magnetron sputtering chamber. When the base vacuum of 4×10^{-6} Torr was attained, high purity argon gas was introduced at a flow rate of 20 SCCM, to sputter Zn metal target (MTI Corporation. USA 99.99%) at DC power of 150 W. The substrate temperature was fixed at 400 °C and the deposition durations were for 15, 30, and 45 s, for which thicknesses were 5, 10, and 15 nm, respectively. We also sputter Zn for 15 s at 200 and 300 °C on the ZnO NWs arrays, which were further annealed at 400 °C in air ambient. The preliminary investigations on the morphology and the crystalline phase were carried by X-ray diffractometer (model Seifert XDAL 3000), field emission scanning electron microscopy (FESEM, model JEOL JSM-6700F) and high-resolution transmission electron microscopy (HRTEM, model JEM 2010). The elemental mapping was also done by the same FESEM system. Photoluminescence at room temperature was measured using a He−Cd laser (Kimmon Koha Co., Ltd.; model KR1801C) with 325 nm excitation source and recording the luminescence using a spectrometer (Horiba Jobin Yvon, Model: iHR 320) together with a photomultiplier tube. Two circular (1 mm diameter) gold electrodes (50 nm thickness) were evaporated through a shadow mask at a separation of 3 mm on the top of the ZnO NWs arrays to measure the current using the Keithley meter (model 2400). The NWs were illuminated with a monochromatic light from a xenon lamp (150 W) fitted with a spectral illuminator system (model 9050, New-port Corp, USA) for 15 min during photocurrent measurement.

RESULTS AND DISCUSSIONS

The scheme of Zn sputtering for Zn diffusion into ZnO NWs is given in Figure 1. The FESEM images (see the Supporting Information, Figure S1a and b) show that the morphology of the NWs before and after Zn sputtering (15 s) does not change as expected from the model. The diameters of the NWs are of the order of 30 nm as shown in the TEM images (see the Supporting Information, Figure S2). We could gather evidence of Zn diffusion from the elemental mapping on a single as-grown and Zn-sputtered ZnO NW. The Figure 2 shows Zn:O ratio in (ratio of the line intensities for Zn and O) as-grown NW is 3:5, whereas that in the Zn/ZnO NW is 13:10. Considering the very small values of the percentage experimental errors (for Zn, O, and Si as 1.36, 0.53, and 0.23, respectively, in the case of ZnO NWs and as 1.40, 0.52, and 0.26, respectively, in the case of Zn/ZnO NWs), the trend can be understood from the EDS results that more Zn is present in the Zn/ZnO NWs. The X-ray diffraction spectrograms for ZnO and 30 s Zn-sputtered ZnO NWs are given in the Supporting Information, Figure S3, which do not show any significant change. Because the amount of Zn is very small, no diffraction peak due to Zn could be detected in the XRD pattern of Zn/ZnO NWs.

Figure 3 shows the room-temperature photoluminescence spectra of the as-grown and Zn/ZnO NWs. Room-temperature PL spectrum of the as-grown ZnO NWs shows a strong UV peak at 380 nm, mainly due to the free exciton (FX) recombination and a broad visible emission ranging from 400−700 nm peaking around 590 nm, which is attributed to the defect related emission. The PL spectrum of the sample, on which Zn is sputtered at 400 °C for 15 s shows a very strong band edge emission whose intensity is more than 6 times compared to that of the as-grown ZnO NWs. However, the peak shows a red shift of 7 nm. With increase in the time of deposition of the sputtered Zn layer (thus thickness is increased) from 15 to 45 s, the intensity of the UV emission decreases. The maxima of the visible emission are also shifted from 587 to 506 nm which means the visible emission shifts mainly from yellow-orange to green one. Our observations on the changes in UV and visible emissions have been interpreted carefully.

The diffusion in a perfect lattice in which all the lattice sites are occupied by the proper ions is quite impossible as the diffused ion finds no place to occupy (23). The diffusion is possible in an imperfect lattice (with interstitials or vacancy type of defects) where migration of the interstitial defects can occur which needs comparatively less energy. In case of ZnO, which has lot of point defects, the activation energies for lattice diffusion of zinc and oxygen are 3.2 and 7.2 eV (24) respectively. However, the status of defects in bulk and 1D NWs is quite different. In the latter, the defects are close to the surface due to the reduced dimension. Thus, easier formation as well as diffusion of the defects may be possible in the Q1D compared to the bulk. The thermal energy (kT) is not sufficient for the lattice diffusion, and thus it is not expected that these would move to the respective lattice sites even in the NWs. Therefore, we consider two possibilities of zinc diffusion producing defects other than sitting in the proper lattice site. First, Zn may diffuse to the Zn vacancy or to an interstitial site decreasing the number of V_{zn} or increasing the number of Zn_i. Second, Zn may migrate to the oxygen vacancy forming the Zn antisites.

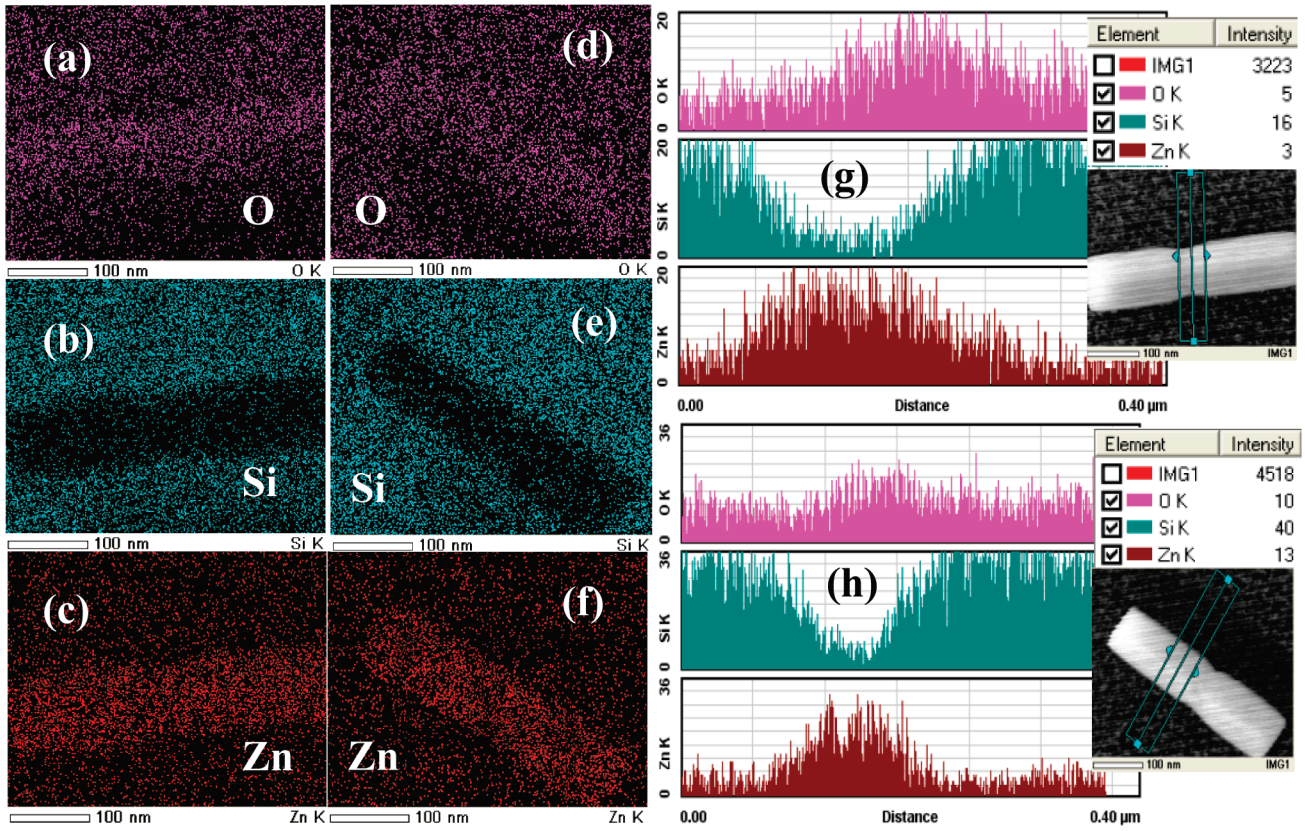

FIGURE 2. Elemental mapping of (a–c) as-grown and (d–f) Zn-sputtered ZnO NW. (g, h) Line intensities corresponding the elements (O, Zn, Si) respectively for as-grown and Zn-sputtered ZnO NWs. The corresponding inset in the figures shows the SEM image and the values of elemental intensities in the NW.

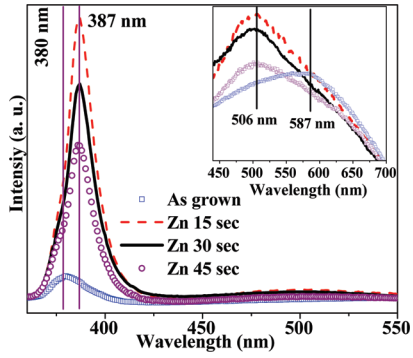

FIGURE 3. Room-temperature photoluminescence spectra of the ZnO NWs and Zn-sputtered ZnO NWs at 400 °C. Inset gives the magnified visible emission spectra of ZnO NWs and Zn-sputtered ZnO NWs.

Another possibility, that excess zinc may form new ZnO, can not be ruled out. Because antisites have extremely high formation energies (16), antisite mediated diffusion mechanism can be excluded in the present case. Before Zn sputtering, the NWs were kept in high vacuum at 400 °C to ensure that there is no more adsorbed oxygen to form new ZnO reacting with Zn. Thus, we would concentrate only on the possibility of Zn_i formation. Depending on the position of Fermi levels in Zn and O-rich conditions, the formation energy of Zn_i may vary from 0 to 6.0 eV and 3.0 to 10.0 eV, which is very high (16). Because of the high formation energy, Zn_i-mediated Zn self-diffusion in ZnO is quite unlikely. However, Zn_i can be formed in n-type ZnO in a nonequilibrium condition (16). Sputtering technique provides nonequilibrium growth conditions and thus Zn_i formation cannot be ignored here. The migration energy of Zn_i being low (0.57 eV) (16), in our case, Zn_i would have very high mobility (because temperature is 400 °C). The low formation but high migration energy (1.4 eV) of V_{zn} (16) together with the fact that V_{zn} (positive ion vacancy) can attract Zn_i easily, causes Zn diffusion, mediated by V_{zn}. This is probable in our case because V_{zn} are likely to exist on the surface of the ZnO NWs (25). Tomlins et al. (26) also suggested that Zn self-diffusion in ZnO is controlled by vacancy mechanism.

Because the ionization energy of Zn_i is of the order of 51 meV (27), newly formed Zn_i can easily be ionized. FX is mobile inside the crystal lattice and may recombine at these Zn_i leaving Zn_i atoms ionized. If the coupling occurs between FX and Zn_i, this should give rise to a PL emission with a red shift comparable to the ionization energy of Zn_i. The red shift of the strong UV emission with 7 nm (59 meV) of the Zn-sputtered NWs indicates that there is some coupling of the free exciton (FX) with the Zn_i. Similar red shift has also been observed in case of electrodeposited Zn–ZnO structure after heating (28). The PL spectra of all the Zn-sputtered NWs in Figure 2 for higher Zn layer thickness (deposited for 30 and 45 s) with 7 nm red shift in the band edge emission confirms coupling of Zn_i and FX. By Zn sputtering, a large number of Zn_i-related defects are formed, and thus the probability of coupling between FX and the Zn_i increases giving rise to an enhanced UV emission. With an increase in the Zn sputtering

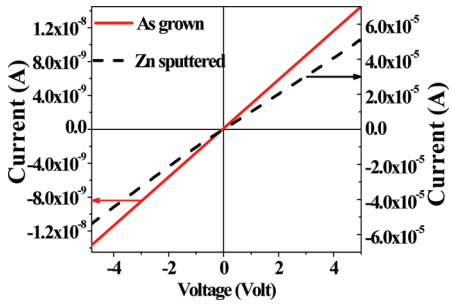

FIGURE 4. (a) $I-V$ characteristics of the as-grown and 30 s Zn-sputtered ZnO NWs.

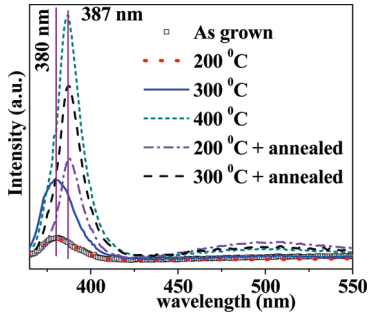

FIGURE 5. Room-temperature PL spectra of the as-grown and 15 s Zn-sputtered ZnO NWs at different temperature and subsequent annealing at 400 °C.

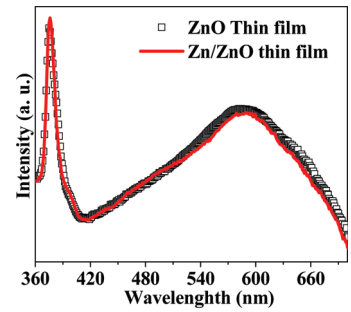

FIGURE 6. Room-temperature PL spectra of ZnO thin film and 30 s Zn-sputtered ZnO thin film.

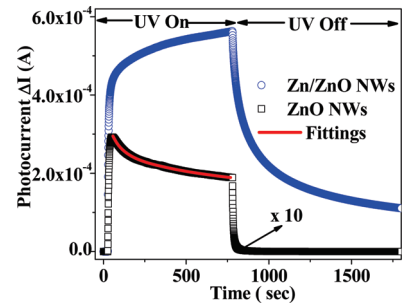

FIGURE 7. Transient photocurrent measurement of the as-grown and the 30 s Zn-sputtered ZnO NWs at 3 V. The solid red line gives the biexponential fittings of the photocurrent decay during steady illumination.

time, the decrease in the intensity of the band edge emission is not understood well at this moment. Now, let us interpret the changes in the defect emission of the Zn-sputtered ZnO NWs. The defect related emissions in nanostructured ZnO have been outlined in details by Djurisic and Leung (29). It was observed earlier that Zn_i (30) causes red emission, V_{Zn} (16) and V_O (31, 32) cause the green emission, and excess oxygen cause the orange-red emission (31). Chen et al. (33) also found that the orange-red emission of the ZnO nanowires is related to the excess oxygen on the ZnO surface, and it is also tunable via annealing and surface modifications. Thus, in our case, the absence of excess O_2 molecules should lead to the reduction of the orange-red emission in contrast to the as-grown sample. This is what we have observed in the PL results. At the same time, evolution of the green emission confirms the formation of V_{zn} related complex defect (25, 34). Considering Zn_i to be the shallow donors in n-type ZnO (11, 12), we should expect an enhanced conductivity in the Zn-sputtered NWs. $I-V$ curve of the Zn-sputtered NWs in Figure 4 indeed shows a drastic increase in the current level by 3 orders of magnitude as anticipated. Thus, the electrical results also indicate that the cause behind the n-type conductivity (in this case, it is presumably Zn_i) is increased as a result of Zn sputtering.

To confirm further, we have sputtered Zn at 200 and 300 °C for 15 s. Figure 5 shows that there is no much change in the intensity and peak position of the excitonic PL emission compared to as-grown unsputtered NWs. However, the intensities of the UV peaks are smaller compared to that of the sample with Zn sputtered at 400 °C. Once these samples are annealed at 400 °C in air ambient, the intensity of the band edge emission significantly increases and a red shift (with 7 nm) has been observed in both supporting our view on the probable coupling of the free exciton with Zn_i. All these results indicate that there is no diffusion of Zn ion into the NWs when the temperature is less than 400 °C because 200 and 300 °C temperatures are not sufficient to diffuse Zn_i.

We have also sputtered Zn on ZnO film of thickness 200 nm grown by RF magnetron sputtering technique under similar deposition conditions at 500 °C substrate temperatures. Interestingly, we have not observed any change in the PL spectrum of Zn-sputtered ZnO film as shown in Figure 6. This indicates that Zn diffusion in ZnO grains has not occurred even at 500 °C temperature,s implying the surface diffusion of Zn is easier in case of the NWs because of the smaller dimension.

The schematic measurement for the photocurrent arrangement using two probe contact is given in the Supporting Information (Figure S4). Figure 7 shows that the transient photocurrent growth and decay of the as-grown NWs and Zn-sputtered (30 s) ZnO NWs by switching "on" and "off" the UV light (360 nm). It is known that the surface adsorbed O_2 and water molecules largely affect the photoresponse of the NWs (19, 20). O_2 molecules chemisorbed and physisorbed on the NWs' surface get ionized as O_2^- by trapping electrons from the NWs that result in the formation of a depletion layer causing a band bending toward upward. This leads to a barrier height for the electrical conduction. On illumination, the photoexcited holes are generated and are trapped by the adsorbed O_2^- through the surface electron–hole recombination; while the photo excited unpaired electrons significantly increase the conductivity due to the increased lifetime (2). From the transient photocurrent spectra it is clear that the maximum photogenerated current,

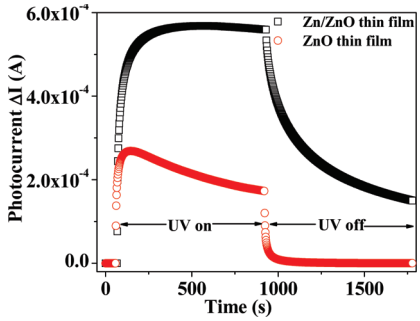

FIGURE 8. Transient photocurrent measurement of the as grown and the 30 s Zn-sputtered ZnO thin films at 5 V.

ΔI_{max} (photocurrent minus dark current) for the Zn-sputtered ZnO is 5.63 × 10^{-4} A, which is almost 20 times higher compared to the ΔI_{max} of the as-grown NWs, which is 2.91 × 10^{-5} A. The higher photocurrent generation can also be explained with the help of coupling between the free exciton and the Zn_i. When UV light is illuminated on the Zn-sputtered ZnO NWs, excitons are generated which then interact with Zn_i to ionize them. Once Zn_i is ionized, it leads to the generation of free electrons in the conduction band, which increases the photocurrent values. The growth time constants are 5.5 and 7 s, respectively, while the decay time constants are 7 and 250 s, respectively, for ZnO and Zn/ZnO. The incorporation of extra defect states leads to the slower response, which also supports our prediction that Zn diffusion occurs in ZnO NWs. The as-grown NWs show steady state photocurrent decay when the UV illumination is on like earlier reports (9, 19). As previously reported (9, 19), the decay is well-fitted with the biexponential decay equation of the type

$$I = I_0 + Ae^{-t/\tau_1} + Be^{-t/\tau_2}$$

where τ_1 and τ_2 are two decay constants. In this case, as-grown ZnO NWs, the values of τ_1 and τ_2 are 60 and 592 s respectively. But interestingly, the Zn-sputtered ZnO NWs also show no photocurrent decay during steady UV illumination. We have already reported that this carrier relaxation can be reduced or eliminated by the surface capping that helps to increase the photocurrents (35, 36). Transient photocurrent spectra of the ZnO thin films (Figure 8) shows a small increase in the photocurrent values for the Zn-sputtered ZnO thin film compared to the as-grown one, which also supports the PL results. The maximum photocurrent values for Zn-sputtered ZnO thin films is 5.68 × 10^{-4} Å and for as-grown ZnO thin films, it is 2.68 × 10^{-4} Å. This observed difference in the photoconductivity in thin films NWs can be explained in terms of the surface to volume ratio. It is well-known that two processes generally govern the UV photoconductivity in ZnO: (1) the surface-related process and (2) the bulk-related process. For the nanoscale materials, when the dimension decreases beyond a certain extent, it is possible that the bulk defects segregates on the surface thereby producing a large difference in the properties. Thus, higher photocurrent generation owing to ionization of Zn_i is observed in the NWs because of the high surface-to-volume ratio. But in case of thin film, the surface to volume ratio is much less compared to the NWs, and thus sputtered Zn cannot diffuse to the bulk. So there is less chance for the change in the photoconductivity of ZnO thin film after and before Zn sputtering.

CONCLUSION

In summary, sputtering of Zn onto quasi-one-dimensional ZnO NWs at 400 °C leads to diffusion of Zn into ZnO NWs. As a result of Zn diffusion, UV emission has been enhanced along with a red shift in the UV peak position in Zn/ZnO NWs. Although Zn sputtering produces no significant change in case of thin films. The photocurrent generation is also enhanced largely after Zn diffusion. The enhancement in both UV emission and photocurrent generation, and the shift in the UV peak position are corelated to the interaction between the free exciton and Zn_i. Zn diffusion in the NWs occurs easily via V_{zn}, because of close proximity of the bulk defects from the surface in the low-dimensional nanostructures. The results are important for optoelectronic applications of ZnO NWs.

Acknowledgment. The authors acknowledge the HRTEM facility created by the Department of Science and Technology (DST), New Delhi under the Nano Initiative program. The authors would like to acknowledge Mr. S. Maji for the measurement of elemental mapping.

Supporting Information Available: FESEM images, HRTEM images, XRD patterns of the as grown ZnO NWs and the 30 s Zn-sputtered ZnO NWs and the arrangement for the current measurement (PDF). This material is available free of charge via the Internet at http://pubs.acs.org.

REFERENCES AND NOTES

(1) Law, M.; Greene, L. E.; Johnson, J. C.; Saykally, R.; Yang, P. D. *Nat. Mater.* **2005**, *4*, 455–459.
(2) Soci, C.; Zhang, A.; Xiang, B.; Dayeh, S. A.; Aplin, D. P. R.; Park, J.; Bao, X. Y.; Lo, Y. H.; Wang, D. *Nano Lett.* **2007**, *7*, 1003–1009.
(3) Gargas, D. J.; Toimil-Molares, M. E.; Yang, P. *J. Am. Chem. Soc.* **2009**, *131*, 2125–2127.
(4) Zimmler, M. A.; Stichtenoth, D.; Ronning, C.; Yi, W.; Narayanamurti, V.; Voss, T.; Capasso, F. *Nano Lett.* **2008**, *8*, 1695–1699.
(5) Lu, M. Y.; Song, J.; Lu, M. P.; Lee, C. Y.; Chen, L. J.; Wang, Z. L. *ACS Nano* **2009**, *3*, 357–362.
(6) Özgür, Ü.; Alivov, Y. I.; Liu, C.; Teke, A.; Reshchikov, M. A.; Doğan, S.; Avrutin, V.; Cho, S. J.; Morkoç, H. *J. Appl. Phys.* **2005**, *98*, 041301.
(7) Kapilashrami, M.; Xu, J.; Biswas, A.; Tamaki, T.; Sharma, P.; Rao, K. V.; Belova, L. *Mater. Lett.* **2010**, *64*, 1291–1294.
(8) Wu, Y.; Tamaki, T.; Voit, W.; Belova, L.; Rao, K. V. *Mater. Res. Soc. Symp. Proc.* **2009**, *1161*, I03–22.
(9) Bera, A.; Basak, D. *Appl. Phys. Lett.* **2008**, *93*, 053102.
(10) Hsu, C. L.; Chang, S. J.; Lin, Y. R.; Li, P. C.; Lin, T. S.; Tsai, S. Y.; Lu, T. H.; Chen, I. C. *Chem. Phys. Lett.* **2005**, *416*, 75–78.
(11) Look, D. C.; Hemsky, J. M.; Sizelove, J. R. *Phys. Rev. Lett.* **1999**, *82*, 2552–2555.
(12) Oba, F.; Nishitani, S. R.; Isotani, S.; Adachi, H.; Tanaka, I. *J. Appl. Phys.* **2001**, *90*, 824–828.
(13) Hofmann, D. M.; Hofstaetter, A.; Leiter, F.; Zhou, H.; Henecker, F.; Meyer, B. K.; Orlinskii, S. B.; Schmidt, J.; Baranov, P. G. *Phys. Rev. Lett.* **2002**, *88*, 045504.
(14) Lee, E. C.; Chang, K. J. *Phys. Rev. B* **2004**, *70*, 115210.
(15) Lavrov, E. V.; Borrnet, F.; Weber, J. *Phy. Rev. B* **2005**, *71*, 035205.
(16) Janotti, A.; Van de Walle, C. G. *Rep. Prog. Phys.* **2009**, *72*, 126501.

(17) Zhao, Q.; Xu, X. Y.; Song, X. F.; Zhang, X. Z.; Yua, D. P.; Li, C. P.; Guo, L. *Appl. Phys. Lett.* **2006**, *88*, 033102.
(18) Kang, H. S.; Kang, J. S.; Kim, J. W.; Lee, S. Y. *Appl. Phys. Lett.* **2004**, *95*, 1246.
(19) Bera, A.; Basak, D. *Appl. Phys. Lett.* **2009**, *94*, 163119.
(20) Li, Q. H.; Gao, T.; Tang, Y. G.; Wang, T. H. *Appl. Phys. Lett.* **2005**, *86*, 123117.
(21) Lee, M. K.; Tu, H. F. *Jpn. J. Appl. Phy.* **2008**, *47*, 980–982.
(22) Igasaki, Y.; Saito, H. *Thin Solid Films,* **1991**, *199*, 223–230.
(23) Dekker, A. J. *Solid State Physics* 1957, Prentice-Hall.
(24) Gupta, T. K.; Carlson, W. G. *J. Mater. Sci.* **1985**, *20*, 3487–3500.
(25) Tam, K. H.; Cheung, C. K.; Leung, Y. H.; Djurisic, A. B.; Ling, C. C.; Beling, C. D.; Fung, S.; Kwok, W. M.; Chan, W. K.; Phillips, D. L.; Ding, L.; Ge, W. K. *J. Phys. Chem. B.* **2006**, *110*, 20865–20871.
(26) Tomlins, G. W.; Routhbort, J. H.; Mason, T. O. *J. Appl. Phys.* **2000**, *87*, 117–123.
(27) Hutson, A. R. *Phys. Rev.* **1957**, *108*, 222–230.
(28) Lee, M. K.; Tu, H. F. *J. Appl. Phys.* **2007**, *101*, 126103.
(29) Djurisic, A. B.; Leung, Y. H. *Small* **2006**, *2*, 944–961.
(30) Gomi, M.; Oohira, N.; Ozaki, K.; Koyano, M. *Jpn. J. Appl. Phys.* **2003**, *42*, 481.
(31) Teke, A.; Ozgur, U.; Dogan, S.; Gu, X.; Morkocü, H.; Nemeth, B.; Nause, J.; Everitt, H. O. *Phys. Rev. B* **2004**, *70*, 195207.
(32) TekeXing, G.; Wang, D.; Yi, J.; Yang, L.; Gao, M.; He, Mi.; Yang, J.; Ding, J.; Sum, T. C.; Wu, T. *Appl. Phys. Lett.* **2010**, *96*, 112511.
(33) Chen, T.; Xing, G. Z.; Zhang, Z.; Chen, H. Y.; Wu, T. *Nanotechnology* **2008**, *19*, 435711.
(34) Bera, A.; Basak, D. *Chem. Phys. Lett.* **2009**, *476*, 262–266.
(35) Bera, A.; Basak, *ACS Appl. Mater. Interfaces* **2009**, *1*, 2066–2070.
(36) Bera, A.; Basak, D. *ACS Appl. Mater. Interfaces* **2010**, *2*, 408–412.

AM1006047